Two- and three-dimensional confined granular chute flows: experimental and numerical results

2005 J. Phys.: Condens. Matter 17 S2457

(http://iopscience.iop.org/0953-8984/17/24/006)

INSTITUTE OF PHYSICS PUBLISHING JOURNAL OF PHYSICS: CONDENSED MATTER

J. Phys.: Condens. Matter **17** (2005) S2457–S2480 doi:10.1088/0953-8984/17/24/006

Two- and three-dimensional confined granular chute flows: experimental and numerical results

Weitao Bi, Renaud Delannay, Patrick Richard, Nicolas Taberlet and Alexandre Valance

Groupe Matière Condensée et Matériaux, CNRS UMR 6626, Université Rennes 1, F35042 Rennes Cedex, France

Received 16 March 2005
Published 3 June 2005
Online at stacks.iop.org/JPhysCM/17/S2457

Abstract

We present experimental and numerical results on 2D and 3D confined granular chute flows. We address the issue of the role of the lateral boundaries. In particular, we find that the presence of flat frictional lateral walls greatly alters the flow features as soon as the width of the flowing layer is of the order of the spacing between the walls or greater. First, steady and fully developed (SFD) flows are observed up to very large inclination angles where accelerated flows would have been expected. Second, at given inclination angle, there exists an upper bound on the flow rate for SFD flows to occur. When one approaches this critical flow rate, a static heap forms along the chute base, on which is the flowing layer. The heap is stabilized by the flow atop it and was named a sidewall-stabilized heap (SSH) since its angle is much greater than those usually exhibited by granular heaps. Both kinds of flow have been studied in 2D and 3D confined configurations. In particular, it is found that these flows exhibit either a Bagnold velocity profile or an exponential one. Moreover, we identify a dimensionless parameter, depending crucially on the sidewall friction, that is expected to drive the transition between these two regimes. We also point out the differences between purely 2D flows and 3D confined flows.

(Some figures in this article are in colour only in the electronic version)

1. Introduction

Granular material flows on inclined chutes still pose some challenging problems related to modelling. Unlike classical fluids, which are correctly described by Navier–Stokes equations, there is no complete and general theory for the description of granular fluids.

Depending on velocity, granular flows are usually divided in three classes: rapid flows where particles interact collisionally, quasi-static flows where particles have enduring contacts and dissipate energy by friction, and an intermediate regime in between (dense flow regime) where both enduring frictional contacts and collisions play important roles. While rapid flows

are correctly described by kinetic theories [1] and quasi-static flows by soil plasticity models, dense flow regimes resist modelling, and no sound convincing constitutive law is available.

In this paper, we are concerned with dense granular flows down rough inclines that are encountered in both geophysical and industrial contexts, and we focus specifically on steady and fully developed (SFD) flows. Since a huge experimental [2–7] and numerical [8–10] literature exists on this topic, we find it worthwhile to recall the main outcomes. (i) At a given inclination, SFD flows can be sustained only if the thickness of the flowing layer is greater than a critical height $h_{\rm stop}$ [7]. The height $h_{\rm stop}$ decreases with increasing inclination angles. It can be seen also as the thickness of the deposit remaining on the incline once the flow stops and depends of course on the flowing material and the roughness conditions. Experimental and numerical measurements of this critical curve $h_{\rm stop}$ carried out for different materials and rough bottoms give the same shape, which can be fitted by

$$\frac{h_{\rm stop}(\theta)}{d} = B\frac{\tan\theta_2 - \tan\theta}{\tan\theta - \tan\theta_1} \tag{1}$$

where θ_1, θ_2 and B are fit parameters depending on the experimental system, and d is the diameter of the grains. It is worth noting that θ_1 is the minimum angle where SFD flows can be sustained and θ_2 corresponds to the critical angle for which $h_{\rm stop}$ vanishes. In the flowing regime (i.e., when $h > h_{\rm stop}$), the flow is steady and fully developed for moderate inclinations but accelerates along the incline for too large inclinations (typically for $\theta > \theta_2$) [5, 9, 11]. (ii) Numerical and experimental studies tend to show that the flow velocity roughly exhibits a Bagnold profile:

$$u(y) = u_h[1 - (1 - y/h)^{3/2}] \tag{2}$$

where u_h is the velocity at the free surface $y = h$. In addition, it is found that u_h (or equivalently the mean flow velocity U) scales as

$$u_h \propto U \propto \sqrt{gh}\frac{h}{h_{\rm stop}}. \tag{3}$$

Consequently, the flow rate Q varies as $h^{5/2}$ since $Q \propto Uh$. However, it is worth noting that at low angles of inclination, the velocity deviates significantly from a Bagnold profile and is not far from a linear one. (iii) Simulations show that the velocity fluctuations increase with the inclination angle. The profiles exhibit two extrema, one close to the bottom, the other close to the free surface, while in the bulk, the fluctuations gently decrease [21, 12]. (iv) The packing fraction within dense flows remains remarkably constant, except close to the free surface and the bottom. This constant value appears to be rather independent of the flow thickness but decreases with increasing inclination angle. This feature is common to both experiments and simulations [9, 10, 12, 13].

The above features describe dense granular flows down rough inclines where lateral walls are absent or sufficiently far apart, playing therefore a minor role. Among these features, we will retain three essential ones, namely a Bagnold velocity profile, a discharge law $Q \propto h^{5/2}$ and a constant packing fraction in the core, to define what we will call the 'Bagnold rheology'.

In this paper, we address the issue of the role of the lateral boundaries and its effects on the flow properties. We report on experimental and numerical studies both in 2D and 3D configurations. We found that flat frictional lateral walls alter the flow properties as soon as the width of the flowing layer is of order of or greater than the spacing between the walls. First, SFD flows on rough bottoms are observed up to large inclination angles where accelerated ones are usually expected. Second, at a given inclination angle, there is an upper bound on the flow rate for SFD flows to occur on the rough bottom of the chute, and when one approaches this critical flow rate, a static heap forms along the chute base, on which the material is flowing.

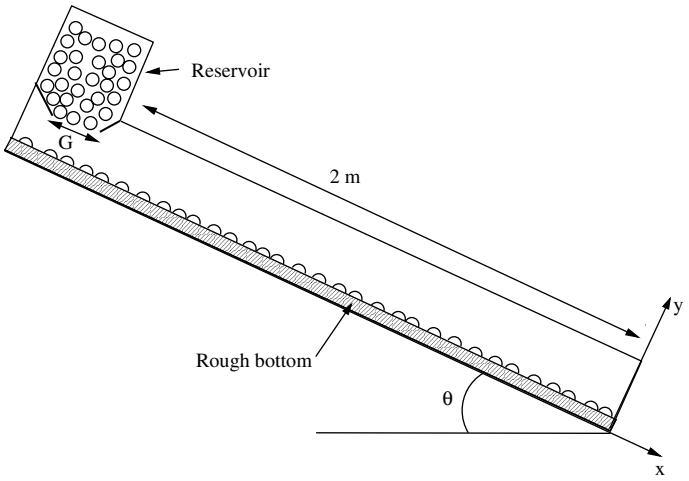

Figure 1. Experimental set-up.

The heap is stabilized by the flow atop it and was named a sidewall-stabilized heap (SSH) since it has a slope angle much greater than those usually exhibited by granular heaps [14–16]. Flows atop an SSH differ from the former flows in the sense that they occur over erodible bottoms but still display steady and fully developed features. We studied the properties of these two kinds of flow (namely, the flows on rough bottoms and the flows atop an SSH) in both 2D and 3D configurations.

The paper is organized as follows. Section 2 is exclusively devoted to 2D experiments where both types of flow are investigated. In the first part of section 2, SFD flow features (packing fraction, translational and rotational velocity as well as velocity fluctuations) are analysed while varying the flow rate and the inclination angle. Flows on an SSH are briefly described in the last part of section 2. Section 3 deals with experimental and numerical investigations of 3D confined chute flows. In particular, the effect of the sidewall friction on the flow properties is carefully analysed. Finally, a conclusion and outlook are given in section 4.

2. 2D granular chute flows

2.1. Experimental set-up

The 2D chute flow experiments were conducted using the set-up illustrated in figure 1. The chute is 2 m long and is made of two sidewalls separated by a gap of 3.3 mm. The flowing particles are 8 mm diameter and 3 mm thick polystyrene white discs. A black ribbon-like mark was printed on each disc to monitor its rotation. The bottom of the chute is made rough by gluing half discs on a smooth base. The half discs were displayed randomly with an interdistance evenly distributed between 0 and $(\sqrt{3}-1)d$. The value $(\sqrt{3}-1)d$ corresponds to the critical situation where a flowing disc fills up the void between two consecutive glued discs. The upper part of the chute is used as a reservoir and can store up to 7200 particles. With this set-up, one can control the flow rate (by adjusting the size G of the opening gate of the reservoir; see table 1) and the inclination angle of the chute tuned through a hydraulic jack.

The granular flows were recorded by a high speed video camera at a rate of 500 images per second and a resolution of 512 × 240 pixels. The observation window is approximately

Table 1. Correspondence between the flow rate Q and the size G of the opening gate of the chute reservoir.

Size of the opening gate, G	5d	7d	9d	11d	13d	15d
Flow rates, Q (particles s^{-1})	209 ± 14	391 ± 12	637 ± 30	913 ± 40	1234 ± 44	1604 ± 54

31 cm $\times$ 15 cm in size and is located 30 cm away from the end of the chute, that is, far enough from the beginning of the chute in order that the flow can reach a steady and fully developed state and not close to the exit to avoid the outflow acceleration. The particle tracking was performed using a sophisticated code we have developed [17]. The error made in the disc position was estimated to 0.1 pixel (i.e., 0.065 mm) and that of disc rotation was about 1°.

Some factors, such as humidity and dust, were found to seriously influence the granular flow properties. Therefore, the experimental set-up was placed in an air-conditioned room and the relative humidity was kept around 50%. Moreover, the lateral walls of the chute were regularly cleaned to avoid accumulation of dust.

2.2. Particle interaction forces

When particles flow in the chute, they interact via binary or multiple collisions and enduring contacts. We have evaluated the coefficient of normal restitution e for binary collisions occurring in the chute flow. We found an average value of 0.57 with a standard deviation of 0.14 for relative impact velocities ranging from 0.15 to 1 m s^{-1}.

Moreover, particles experience air drag and sidewall friction. For particles in the bulk where the flow is relatively dense, air drag is negligible because, as particles entrain air efficiently, the relative velocity between air and particles is drastically reduced. Sidewall friction is important, and it drastically slows down the flow. However, its precise evaluation is rather delicate because it depends greatly on how disc particles come in contact with sidewalls (see [17]).

2.3. General description of the different flow regimes

Steady and fully developed flows were found within a limited range of the flow rate Q and chute inclination θ, as shown in figure 2. At a fixed inclination angle θ, there is an upper bound on the flow rate Q for SFD flows to occur. When one approaches this critical flow rate, one observes a new type of flow. A static heap gradually forms along the chute base: some of the flowing particles get trapped and contribute to the growth of the static heap which eventually stops. The rest of the grains form a flow of uniform width atop the heap. This static heap is stabilized by the flowing layer and can reach therefore angles much higher than the angle of repose. Flows atop an SSH differ from the former flows since they occur over an erodible bottom. As will be shown below, sidewall friction plays a crucial role in the formation of an SSH. It should be noted that there should also exist a lower bound on the flow rate for SFD flows to develop. However, it was not possible with our set-up to produce such low flow rates.

Flows on rough inclines have been widely described in the phase diagram (h, θ) where h is the height of the flow. As stated in the introduction, it has been shown that there exists a critical height, $h_{\mathrm{stop}}(\theta)$, below which flows cannot be sustained [7]. Because of technical constraints (i.e., small capacity of the reservoir) and large fluctuations of the deposit height along the chute (essentially due to the fact that monosized particles were used), we were not able to determine with accuracy h_{stop} for our system. The main effect of the sidewalls is to increase the values of θ_1 and θ_2 in comparison with 3D extended chute flows. We have estimated in our experiments

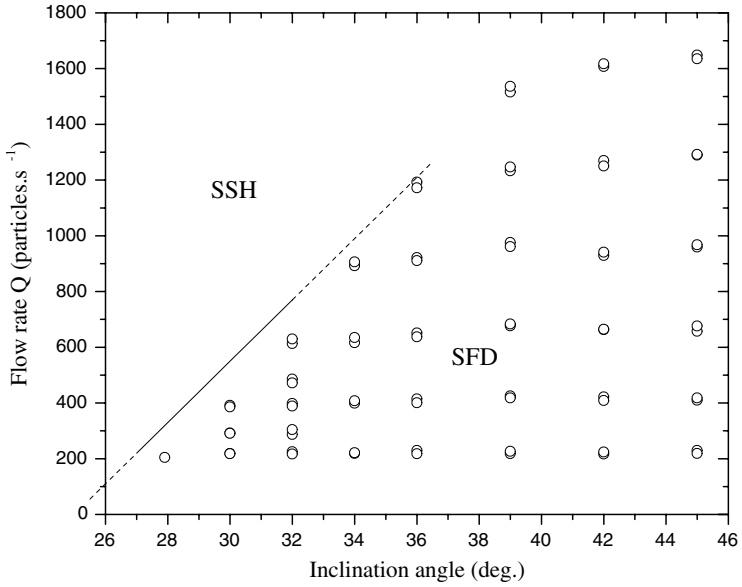

Figure 2. Phase diagram in the control parameter space (Q, θ). The neighbouring symbols correspond to different experiments performed in the same conditions.

the critical inclination angle θ_2 where h_{stop} vanishes, and found $\theta_2 \simeq 32°$. Contrary to 3D extended chute flows where flows are accelerated above θ_2, we can obtain SFD flows on the rough bottom of the chute for angles much greater than θ_2.

2.4. SFD flows on rough bottoms

2.4.1. Packing fraction profile. The most visible behaviour of the flowing particles can be revealed by the packing fraction profiles $\phi(y)$. The profiles are shown in figure 3 for different inclination angles for a fixed flow rate. In the bulk region, the packing fraction is almost constant and exhibits slight oscillations, indicating that the flow is structured in layers parallel to the bed. Close to the free surface, $\phi(y)$ is less structured and decreases rapidly. The average packing fraction in the bulk is close to the 2D random loose packing fraction 0.78. The constant packing fraction throughout the flow is a classical observation for dense granular flows down rough inclines [13].

Additional remarks follow. First, it is worth noting that, for a given flow rate, the height of the flow decreases with increasing inclination angles. This means that the mean flow velocity should increase with increasing inclination angles. Second, it should be noted that the mean packing fraction (averaged over the flow width) slightly decreases with increasing chute inclination (from 0.79 at $\theta = 32°$ to 0.76 at $\theta = 42°$). Furthermore, it does not vary significantly with the flow rate at fixed angle. Similar behaviours were reported in numerical simulations [9].

2.4.2. Discharge curve and mean velocity profiles. Previous experiments on 3D granular flows down inclines have employed special techniques to measure the flow depths, and inferred the mean flow velocities from the flow rates [18]. In the present experiments, the mean flow

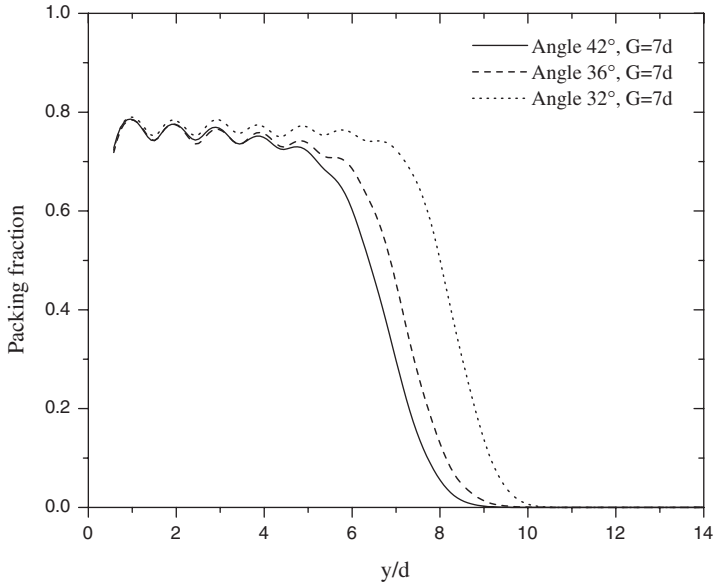

Figure 3. Packing fraction profiles at different inclination angles for a fixed flow rate.

velocities $U(Q, \theta)$ were calculated accurately by

$$U(Q,\theta) = \frac{\int_0^\infty u\phi \,\mathrm{d}y}{\int_0^\infty \phi \,\mathrm{d}y} = \frac{(\pi d^2/4)Q}{\int_0^\infty \phi \,\mathrm{d}y}, \tag{4}$$

and the height of the flow was defined by

$$h = \frac{\int_0^\infty \phi \,\mathrm{d}y}{0.78}, \tag{5}$$

where 0.78 is the random loose packing fraction. It is worth noting that there are other ways to define the height of the flow which would give similar results. One can use, for example, a definition based on a packing fraction cut-off (i.e., $\phi(y = h) = \phi_{\text{cut-off}}$). However, the definition adopted here has the advantage of providing us with a conserved quantity which gives a measure of the number of particles throughout the flow in terms of a width.

The discharge curves $U(Q)$ and $h(Q)$ show some general and important properties of the measured flows (see figures 4(a) and (b)). The mean flow velocity at a fixed inclination angle displays a power law scaling with the flow rate: $U \propto Q^n$. The scaling exponent n increases slightly with the inclination angle and seems to approach a unique limit $1/2$. The value $n = 1/2$ seems therefore appropriate to characterize the general discharge relation of the investigated granular flows. The estimation is different from Bagnold scaling of $n = 3/5$ but falls into the 'Regime A' proposed by Ancey where the granular flow exhibits a small depth and a fairly linear velocity profile [18]. The flow depth h scales with the flow rate Q as a conjugate of $U(Q)$ (because $Q \propto Uh$). The scaling exponents are close to 0.5, and consequently the mean flow velocity is approximately proportional to the flow depth. The linear relation between U and h differs from the Pouliquen $3/2$ power law [7].

The mean streamwise velocity profiles for different flow rates are shown in figure 5. The velocities normal to the streamwise direction are too small to be considered seriously. The profiles reveal that the shear rates near the base are quite constant when the flux varies. Increasing the flow rate tends to extend the region of constant shear. While a linear profile is

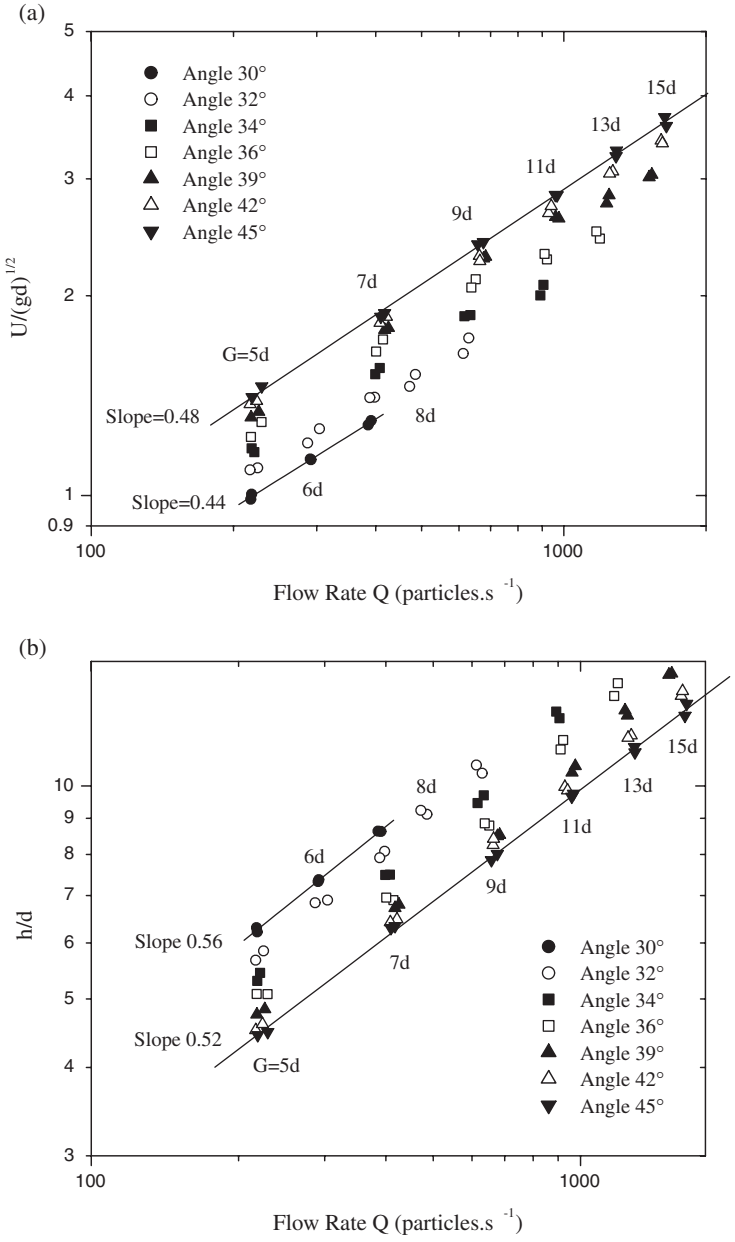

Figure 4. Discharge curves: (a) mean flow velocity; (b) flow depth.

possible for the lower part of deep flows, a Bagnold profile [9] seems to work better globally. It should be pointed out that the parameters in the Bagnold profile were not estimated by fitting, but estimated from the value of the velocity u_h at the height h (defined by $h = \int_0^\infty \phi \, \mathrm{d}y/0.78$). Renormalizing the data by the flow depth h and the surface velocity u_h, we find a good collapse onto the Bagnold profile, as displayed in the inset of figure 5. Near the base, the flow behaves as $u \propto u_h(y/h)$; therefore the invariability of shear rate with flux requires $u_h \propto h$, which is indeed true, recalling the linear scaling between the mean flow velocity and the flow depth.

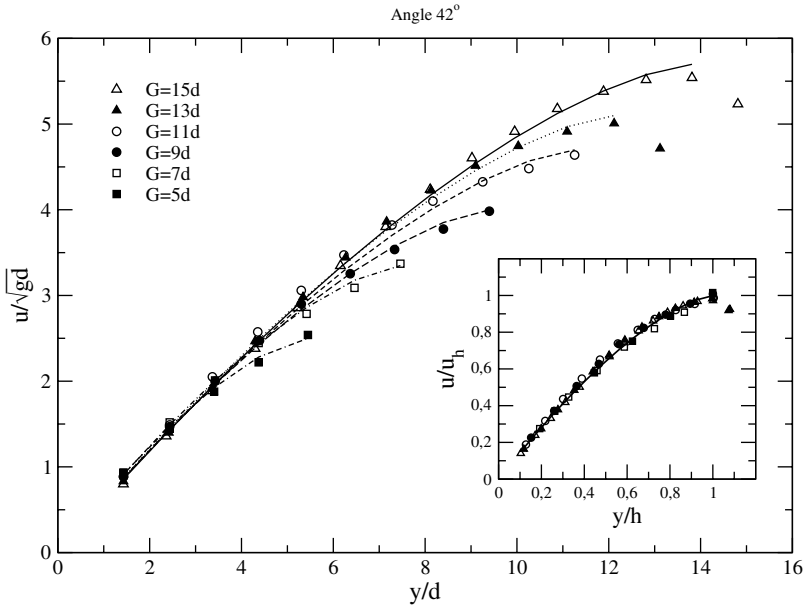

Figure 5. Mean velocity profiles at different flow rates. The Bagnold profile is defined by $u = u_h[1 - (1 - y/h)^{3/2}]$. In the inset, the data are normalized by the flow depth h and the corresponding surface velocity u_h. The different curves correspond to Bagnold profiles.

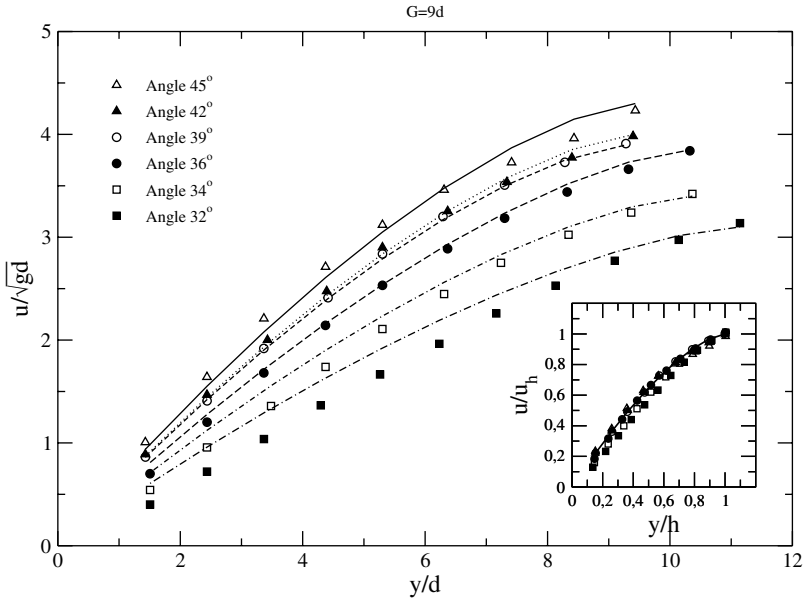

Figure 6. Mean velocity profiles at different inclination angles. In the inset, the data are normalized by the flow depth h and the corresponding surface velocity u_h. The different curves correspond to Bagnold profiles.

The variation of velocity profiles with respect to inclination angles at a fixed flow rate is shown in figure 6. Generally, increasing inclination angle increases the mean shear rate

and results in an increasingly concave profile. At small angles, the velocity profiles are not far away from linear, and hence slightly deviate from the Bagnold profile (inset of figure 6). The shear rates near the bottom (i.e., which is proportional to u_h/h) vary from $0.34\sqrt{gd}$ to $0.54\sqrt{gd}$ for inclination angle ranging from 32° to 45°. At a fixed flow rate, the mean shear rate u_h/h depends therefore on the inclination angle.

At this stage, an important remark should be made. The mean velocity profiles significantly deviate from a linear law only in the upper part of the flowing layer, where precisely the packing fraction starts to decrease. Therefore, if one considers only the part of the flow where the packing fraction is constant, it is tempting to argue that the velocity profile remains linear.

2.4.3. Mean angular velocity profiles. We have also determined the mean angular velocity profiles. According to the kinetic theories [19, 20] the mean angular velocity is related to the rotation rate across the flow depth by

$$\omega = -\frac{1}{2}\frac{\mathrm{d}u}{\mathrm{d}y}. \tag{6}$$

The angular velocity profiles are therefore presented in terms of the relative difference between the angular velocity and the corresponding shear rate: $(\omega + 0.5\,\mathrm{d}u/\mathrm{d}y)/(\omega - 0.5\,\mathrm{d}u/\mathrm{d}y)$. This quantity vanishes when the angular velocity is equal to the shear rate. As can be seen in figure 7, relation (6) is approximately satisfied for most of the flows throughout the flow depth except close to the bottom and the free surface. One can note that near the free surface the rotation speeds are higher than the corresponding rotation rate whereas they are weaker in the basal layer, at least with the rough bottom used here [17].

2.4.4. Temperature profiles. The fluctuating velocities are characterized by the so-called 'granular temperature'. The streamwise and transverse translational temperatures are respectively defined by $T_u = \langle (u - \langle u \rangle)^2 \rangle$ and $T_v = \langle (v - \langle v \rangle)^2 \rangle$, and the rotational temperature by $T_\omega = (d^2/8)\langle (\omega - \langle \omega \rangle)^2 \rangle$. As discussed above, increasing the flow rate at a fixed inclination angle leads to the growth of a core where the shear rate is almost invariable with respect to the flow rate. The development of the core is clearly revealed in the temperature profile (figures 8(a)–(c)). The temperature profiles consist of three regions: a boundary layer where the granular temperature grows sharply up to a local maximum, a core where the granular temperature drops slowly to a local minimum, and a surface layer where the granular temperature grows sharply again. One can therefore clearly identify the core region as being delimited by the two extrema. The magnitudes of the extrema do not seem to vary significantly when increasing the flow rate. Moreover, the thickness of the core grows with increasing flow rate, whereas the extent of the boundary layer remains almost constant. The 'S' shape of the granular temperature profiles is a feature which was observed in numerous numerical simulations of dense flows down inclines [21, 12, 9, 11, 22]. At last, it should be noted that, in the case of shallow flows, the core does not exist: both extrema vanish and, as a result, the temperature increases monotonically from the base to the free surface.

When the flow rate is fixed, the granular temperatures increase with increasing inclination angle, as can be seen in figure 9. There is also a tendency for the near-bed shape of the temperatures to become increasingly convex so as to form a core. This, combined with the foregoing findings, reveals an overall picture of the evolution of granular temperatures with respect to flow rates and inclination angles. In particular, if the granular flows are very shallow or inenergetic, the temperatures increase monotonically from the base to the free surface. Otherwise, the strong perturbations induced by the rough bottom give rise to a highly

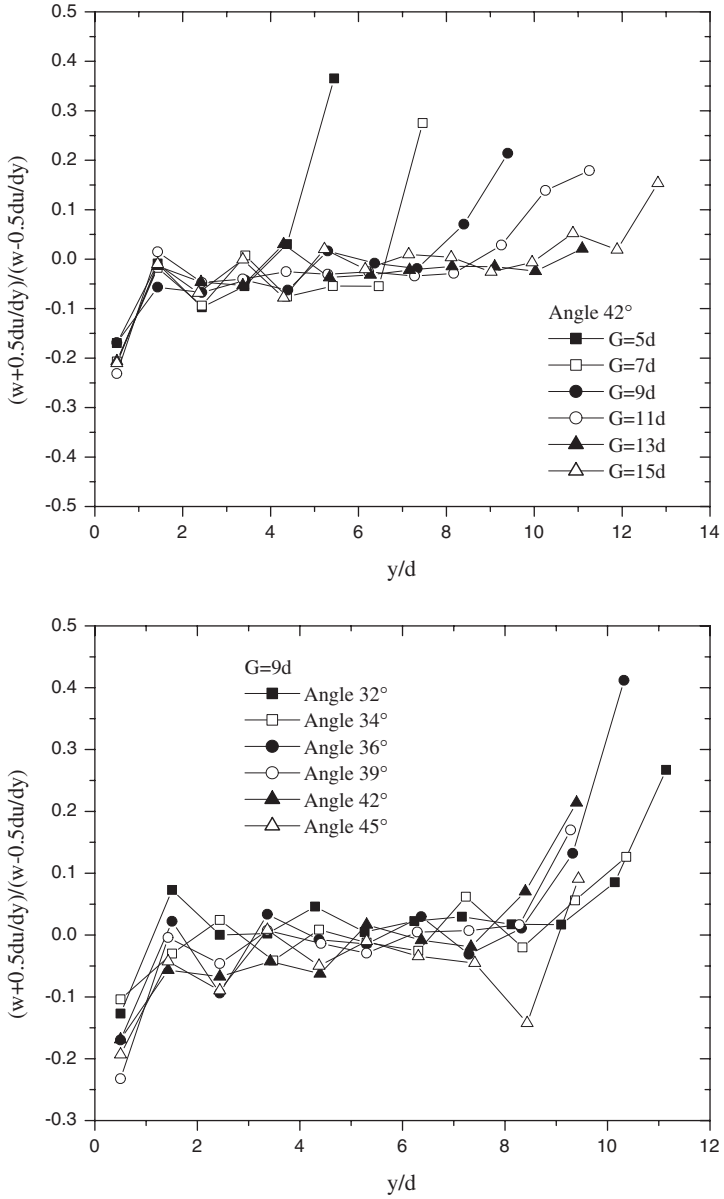

Figure 7. Relative mean angular velocity profiles for different flow rates and inclination angles.

fluctuating region close to the bottom, resulting in an inversion of the kinetic energy flux in the core.

The relative magnitudes of the granular temperatures are shown in figure 10 to reveal the energy partition between the three degrees of freedom. Overall, the temperature ratios T_u/T_v and T_ω/T_v vary only gently with respect to flow rate and inclination angle, except for the basal layer and close to the free surface. Indeed, one can observe in the core region a collapse of the profiles obtained for different flow rates and inclination angles. T_u/T_v is approximately in the range from 1 to 1.2, whereas T_ω/T_v is around 0.5. The flows are weakly anisotropic,

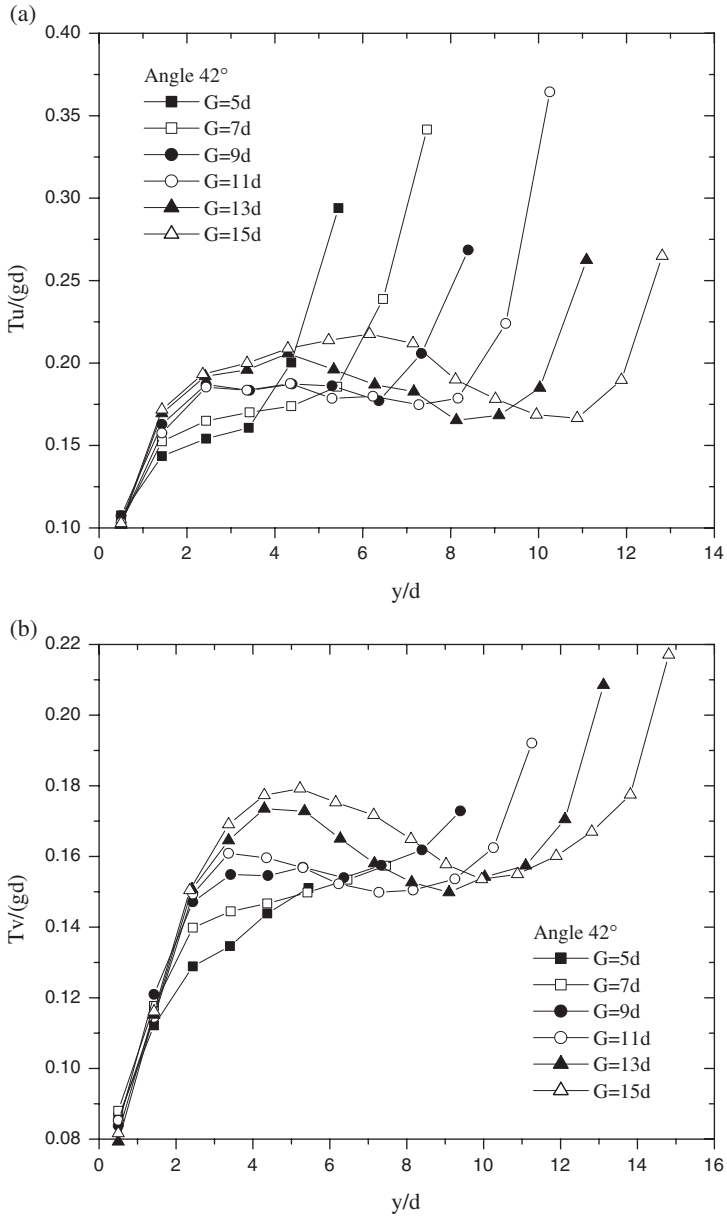

Figure 8. Granular temperatures at different flow rates: (a) streamwise translational temperatures; (b) transverse translational temperatures; (c) rotational temperatures.

and energy is not equally distributed between the rotational and translational modes. These results qualitatively agree with Drake's findings in 2D sphere flows [23]. Quantitatively, they are close to Mitarai's results obtained by numerical simulations on deep 2D disc flows [22].

2.5. Flows on an SSH

As mentioned above, flows on an SSH occur above a critical flow rate which depends on the inclination angle of the chute. For technical reasons (in particular the small capacity of the

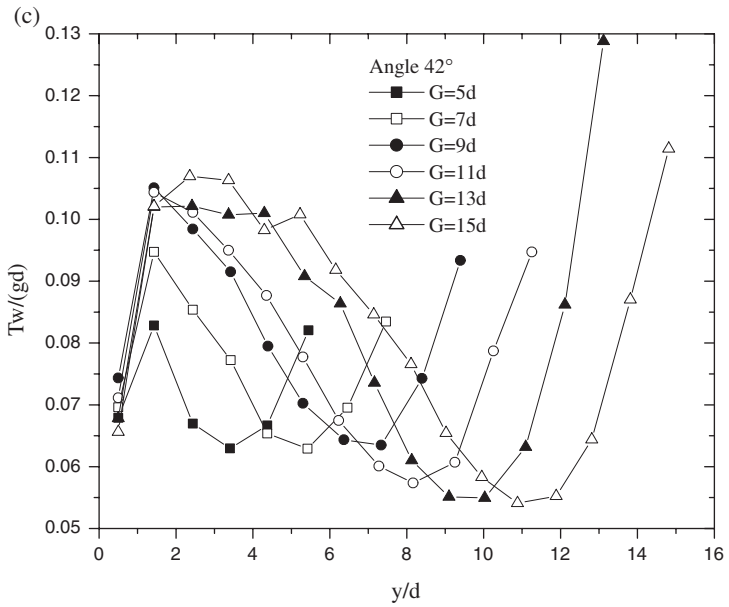

Figure 8. (Continued.)

chute reservoir), we were not able to extensively investigate the properties of flows on an SSH. We present here only qualitative results.

First we have checked that flows atop the SSH are steady and fully developed. We show in figure 11 the velocity profile at different positions along the chute. One can see a superposition of the different profiles giving strong evidence that the flow is fully developed. The shape of the velocity profile bears some strong resemblance with that measured in flows over a static pile or in a rotating drum [24, 25]. One distinguishes two zones: a first zone where the shear rate is seemingly constant (linear part) and a second one where the velocity decreases rapidly (at an exponential rate) to zero.

We have also analysed the packing fraction profile. It seems that the latter remains rather constant throughout the flow as in the case of the flows on rough bottoms. However, additional experiments are required to check this result. Due to the small capacity of the chute reservoir, it was not possible to sustain steady and fully developed flows on the SSH during a long enough time to extract reliable data. A modification of our set-up to enhance the reservoir capacity is therefore needed for extensive analysis of 2D flows on SSHs.

3. 3D confined chute flows

This section is devoted to 3D flows occurring between two vertical sidewalls. Most of previous studies simply ignore the sidewall effect, arguing that the gap between the two walls is large enough. Here, we present an experimental and numerical study of the effect of the sidewall confinement and friction on the flow properties.

3.1. Experimental set-up

The 3D experimental set-up is equivalent to the 2D one (figure 12(a)). Although the tilt angle of the channel, θ, can range from 0° to 90°, our experiments are conducted in a steep

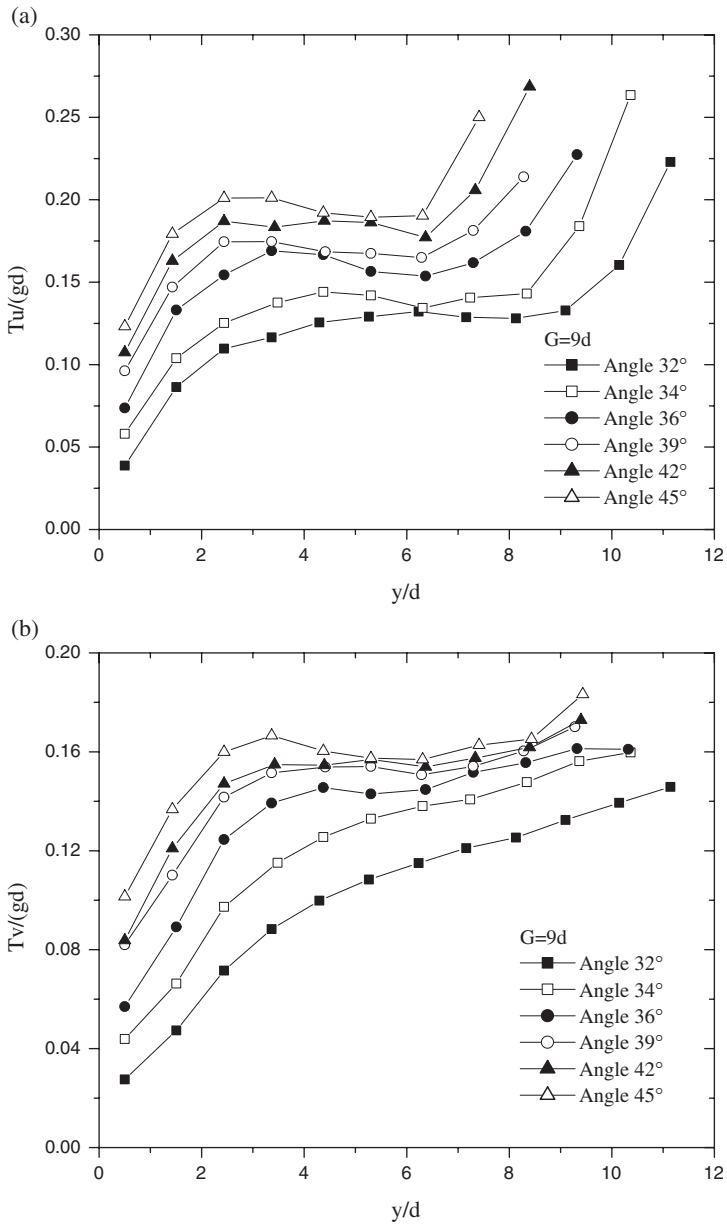

Figure 9. Granular temperatures at different inclination angles: (a) streamwise translational temperatures; (b) transverse translational temperatures; (c) rotational temperatures.

configuration in which θ is always set to be higher than the angle, θ_2, at which all the grains flow out of the channel after the feeding is cut off. Experiments are performed with both dry polydisperse beach sand (0.1–0.8 mm) and slightly polydisperse glass beads (0.6–0.9 mm). Granular material is continuously poured on a rough bottom placed between two transparent vertical glass plates through a hopper whose aperture precisely controlled the input flow rate Q_{in} defined as the mass of material entering the channel per unit of time and per unit of width

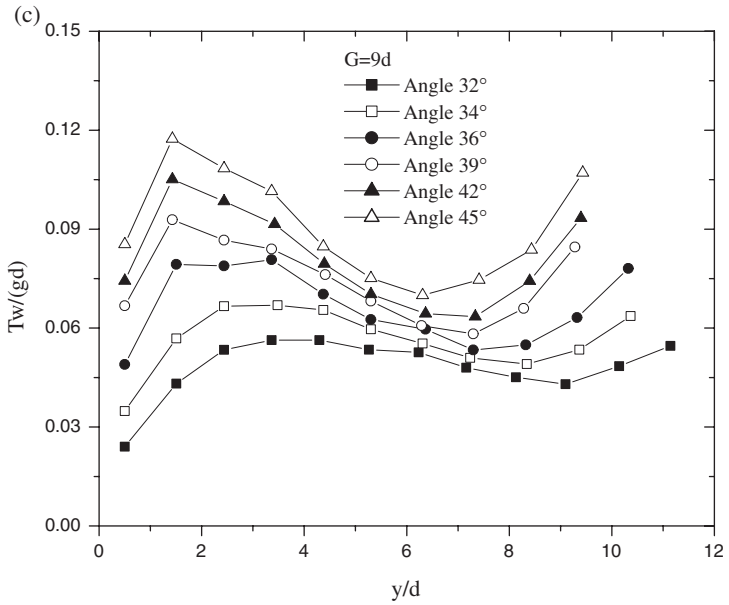

Figure 9. (Continued.)

($Q_{\text{in}} = \text{mass}/(\text{time} \times W)$). In the case of high flow rates the flow can occur at an angle higher than θ. In this regime the angle of the free surface (and of the flow) is called φ. The rough bottom is made of grains (sand or glass beads) glued to a flat rigid substrate. The gap between the two vertical plates W is varied from 5 mm up to 2 cm. The length of the channel is 50 cm and the opening of the hopper is placed 20 cm above the rough bottom, avoiding any feedback interaction between the input flow and the flow in the channel, therefore allowing the feeding rate, Q_{in}, to be tunable and to remain constant throughout an experimental run. As in 2D, all our experiments are conducted in a temperature and humidity-controlled room (24° and 55% humidity). In order to minimize electrostatic effects, the material is passed through a metal sieve connected to the ground prior to all experiments. The angles are measured using an image processing software, leading to a 0.2° uncertainty. The output flow rate, Q_{out}, is determined using an electronic scale which weighed the material falling out of the channel. A fast camera takes pictures at the rate of 8000 frames per second which allows us to perform particle tracking.

3.2. Numerical methods

Numerical simulations are performed using the molecular dynamics (MD) method, also known as the discrete element method (DEM). This method deals with soft (but stiff) frictional spheres colliding with one another. Although not flawless, this type of simulation has been widely used in the past two decades and has proven to be very reliable [26]. The forces acting on the grains are computed and the equations of motion (displacement and rotation) are integrated using the Verlet method. Different normal force models are employed: $F_{ij}^n = k_n \delta_{ij}^{\alpha} + \gamma_n \partial_t \delta_{ij}$, where k_n is a spring constant, δ_{ij} the overlap between two colliding particles, γ_n a viscous damping constant and α a positive number. Two different values of α are used. The Hertz law ($\alpha = 3/2$) is well-suited for collisions of spheres, whereas the spring scheme ($\alpha = 1$) corresponds to collisions of discs. However, $\alpha = 1$ is often used even in the case of spheres for technical

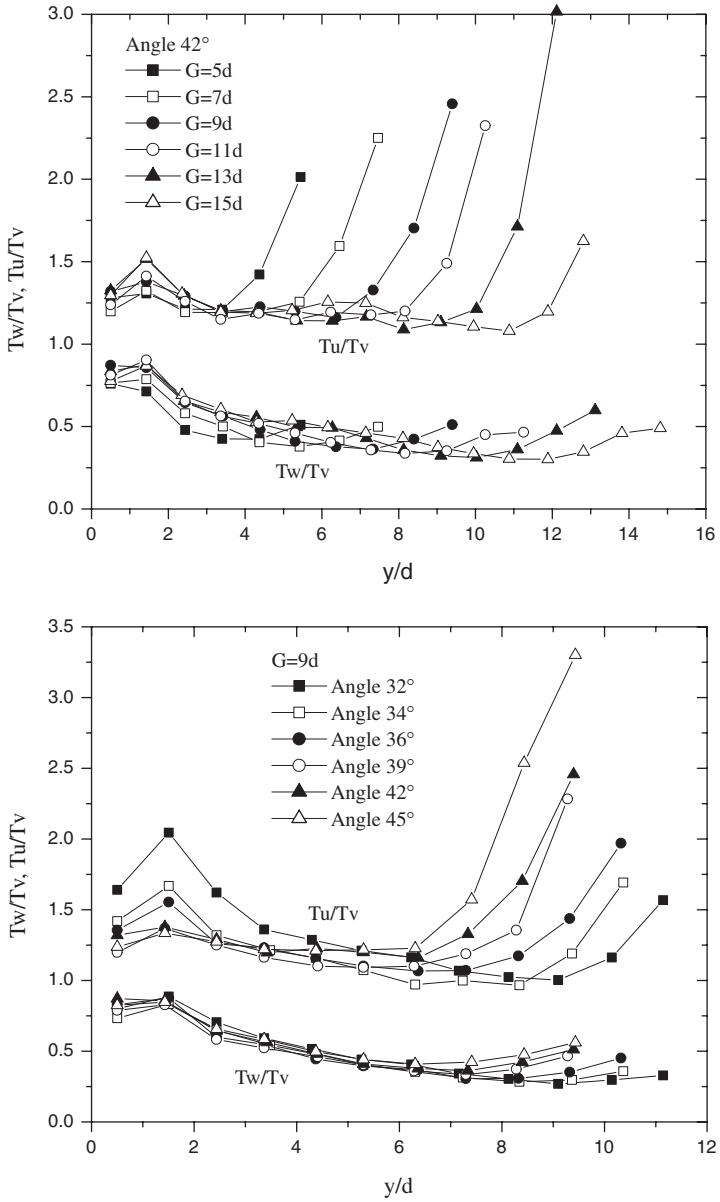

Figure 10. Profiles of temperature ratios T_u/T_v and T_ω/T_v for different flow rates and inclination angles.

reasons [26]. Both schemes were tried in our simulations and produced qualitatively as well as quantitatively similar results. Therefore, the simulations presented here were performed using the spring-like force scheme. Two schemes are also used for the tangential force, F^t. The first one is the regularized Coulomb law: $F^t_{ij} = \min(\mu F^n_{ij}, \gamma_t V^s_{ij})$, where μ is a friction coefficient, γ_t a viscous regularization constant and V^s_{ij} the sliding velocity of the contact. The second one is history dependent: $F^t_{ij} = \min(\mu F^n_{ij}, k_t \Delta_{ij})$, where k_t is a tangential spring constant, Δ_{ij} the tangential displacement. The former is easier to use but the latter is well-suited for

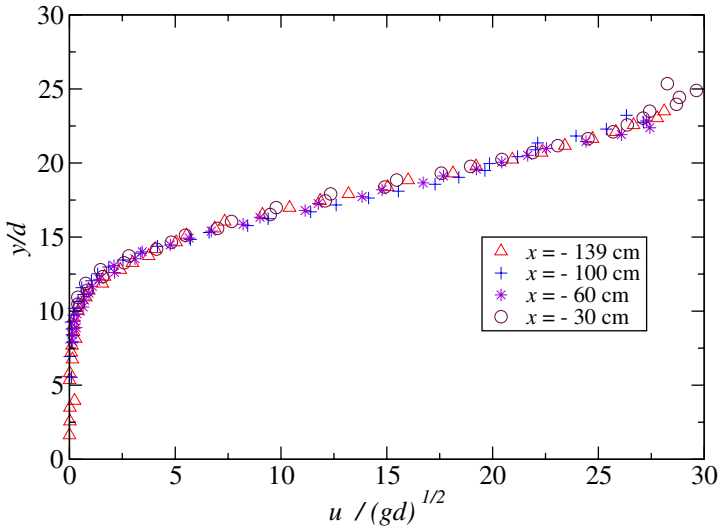

Figure 11. Velocity profiles on an SSH at different streamwise positions x. $G = 8d$ and $\theta = 30°$. Note that $x = 0$ corresponds to the exit of the chute.

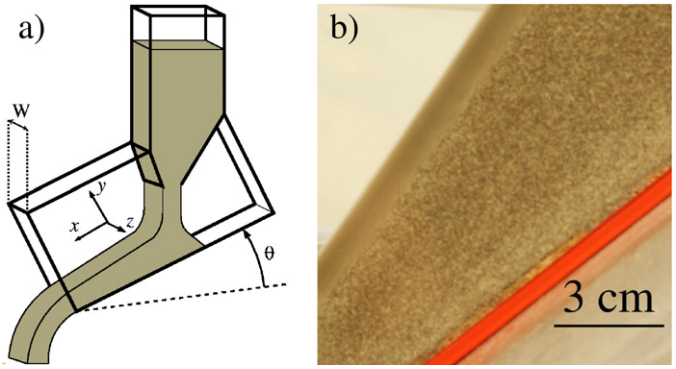

Figure 12. (a) Sketch of the experimental set-up. The granular material is poured from a hopper onto a rough bottom between two vertical plates. (b) Snapshot of the flowing sand taken with a regular video camera with 1/30 s exposure time. The blurry part corresponds to the flowing part.

static piles. Both methods lead to similar results. The following values of the parameters are used: particle diameter $d = 8$ mm, mass $= 0.16$ g, $k_n = 40\,000$ N m^{-1}, $k_t = 10\,000$ N m^{-1}, $\gamma_n = 1.0$ kg s^{-1}, $\gamma_t = 5$ kg s^{-1} and $\mu = 0.8$. For further detail, see [26] for a comprehensive description of all the different force schemes used in granular MD simulations. The above-mentioned values of the parameters lead to a restitution coefficient $e = 0.4$. This value is rather small, but the flow properties were found to be for most part independent of e. Different values of the latter were tried but affected only very dilute flow (typically the gaseous ballistic layer that can appear near the free surface). As expected, the properties of dense flows are not affected, since in dense assemblies of grains the effective coefficient of restitution is close to zero, regardless of the material properties [27].

Two different simulations are used and shown to be equivalent. The first one simulates the whole experimental channel (see figure 12(b)) and will be referred to as the full system (FS).

The second consists of a cell which is made periodic in the direction of the flow. It will referred to as periodic boundary conditions (PBC). Grains are placed in a box with the same bottom and sidewalls as in the FS case. Initially, the grains have no velocity. The cell is then inclined at the angle φ, which triggers a flow that evolves freely toward a steady state for a very wide range of angles (from 38° to 65°). When the angle exceeds a critical value (>65° here) the grains accelerate constantly, whereas the flow comes to rest when the angle is lower than another critical value (<38° here). Note that these values are functions of the simulation parameters and of the channel width. In both systems, Q is measured by counting the number of grains flowing through a surface perpendicular to the sidewalls per unit of time. The bottom is made of cylinders of particle radius placed perpendicularly to the main direction of flow. The gap between two neighbouring cylinders is of 0.5 radius. The walls are flat and frictional and the collisions against them are treated like particle–particle collisions with one of the particles having infinite mass and radius, which mimics a large flat surface. However, it is possible to change the frictional properties of the wall regardless of the value of the particle–particle interaction. The granular material is made slightly polydisperse (±20% in size) in order to avoid crystallization. Our simulations contain a very large number of particles, between 10^5 and 10^6, and run for typically 10^7 time steps. The length, L, of the PBC system must be greater than the typical correlation length. Several system lengths were tried and we observed that for the parameters investigated so far, when $L > 10d$, there is no influence of L on the flow properties. Therefore, all the PBC simulations were run using $L = 25d$.

3.3. Phenomenon: sidewall-stabilized heaps or super-stable heaps (SSHs)

For low flow rates we observe classical flows on the rough bottom of the channel but a new regime, similar to that observed in 2D, occurs for high flow rates [14, 15]. In the latter case, a static wedge-like heap gradually forms [15]: some of the flowing grains get trapped and contribute to the growth of the static heap. The rest of the grains form a steady and fully developed flow that occurs on this heap. Figure 13(a) displays the velocity profile measured at the wall for a system of glass beads, at a distance of 20 cm from the channel exit. As in the 2D case, it shows a seemingly linear part in a region close to the free surface ($0 < y < 30d$), whereas deeper in the pile ($y < 0$), the velocity falls to small but non-zero values. In the latter region, as in flows on a static sand pile, the velocity follows an exponential law [24]. The levelling off at the free surface is typical of a dilute gaseous flow in which trajectories are ballistic. The inset in figure 13(a) displays the velocity profile at the free surface (i.e., seen from above) and shows that the flow is a plug-type flow (high slip velocity at the walls and low shear in the z direction). This indicates that the velocity measured at the wall can be identified with the actual velocity of the whole slab of material. Figure 13(b) displays the velocity profile obtained in PBC simulation (the FS simulation gives identical results). The velocity is averaged over the x and z directions and time. The very good agreement obtained for the profiles demonstrates the reliability of the numerical method. A more careful analysis of the velocity profile reveals in fact that the whole profile (except for the gaseous part) is exponential-like. The height h of the flow will be defined as the depth at which the tangent to the velocity profile (taken at the free surface) intersects the y axis. (Note that the free surface is defined as the boundary between the dense flow and the gaseous part; see figure 13.) The y coordinate origin was set at the depth h, so that the fast flowing part corresponds to positive y, and the slowly decreasing part to negative y.

Let us mention here that although the flow is uniform when averaged over time, there can exist local fluctuations of the flow height, h, sometimes corresponding to upstream traffic waves described in [28, 15]. When the feeding is cut off, the heap slowly erodes and falls apart. This

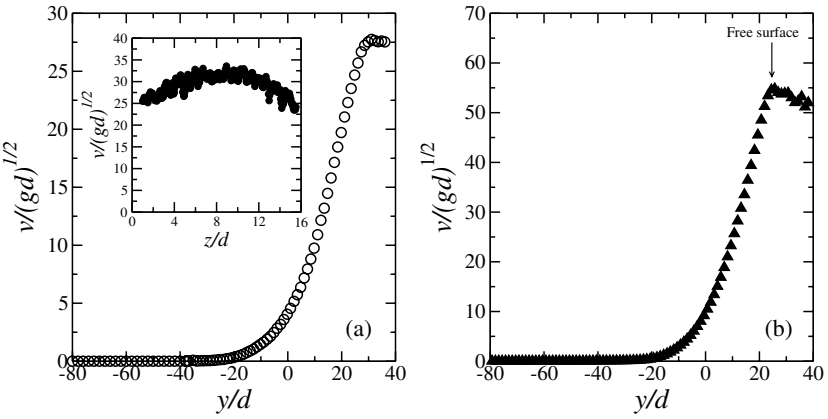

Figure 13. (a) Velocity profile obtained experimentally at the walls for a system of 0.8 mm diameter glass beads and for $W = 12.5$ mm $\simeq 15.5d$, $Q = 90$ g s^{-1} and $\theta = 40°$. The inset presents the velocity at the free surface. (b) Velocity profile obtained numerically using the PBC simulation (see text for details) for $\varphi = 45°$ and $W = 20d$.

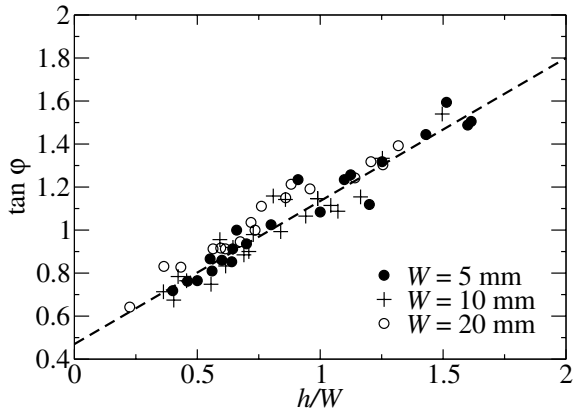

Figure 14. The tangent of the angle φ is plotted as a function of h/W, for different values of the channel width W using polydisperse beach sand. The dashed line corresponds to the fit of the experimental data.

shows that the heap is dynamically stabilized by the flow at its top. One remarkable feature exhibited by such heaps, as in 2D, is their unusual steepness (up to 60° in our experiments) and this is why they are referred to as sidewall-stabilized heaps. For given values of $Q_{\rm in}$ and W, the system 'chooses' an angle φ for the free surface and the corresponding height of the flow h. φ and h depend only on the input flow rate, $Q_{\rm in}$, and on the channel width, W, and not on the tilt angle θ nor on the channel length, L. A simple depth-averaged model [14] provided us with a simple law linking the height of the flow, the angle of the SSH in the final steady state and the channel width. The momentum balance leads to

$$\tan\varphi_\infty = \mu_i + \mu_w \frac{h}{W} \tag{7}$$

where μ_i and μ_w are two effective friction coefficients.

Figure 14 is a plot of φ versus h/W, obtained for different values of the control parameters Q, θ and W. The data fall on a linear curve and then show a good agreement with equation (1)

which indicates that, for the range of h/W (limited by technical constraints) we observed, the solid friction law on the walls describes the phenomenon. For low values of h/d the data deviate from the linear law and reach a plateau. This corresponds to the jamming of the flow. The value of $\tan\varphi$ corresponding to the plateau (for a given channel width) is called μ_{jam} and the height for which $\tan\varphi$ deviates from the plateau h_{jam}.

A best fit to the data provides us with the following values: $\mu_i = \tan(23.3°)$ and $\mu_w = \tan(33.7°)$. One important result of the model is that the relevant parameter to evaluate the effect of the wall friction on the flow is h/W (and not h/d). The model predicts an influence of the sidewall for any given channel width as long as the flowing sand layer is high enough. One can expect the model to break down for flows in very thin channels ($W \lesssim 5d$) where arch effects can play a crucial role. The model may also fail to describe the behaviour of a flow strongly sheared in the z direction. Such a flow can be expected in a channel with very rough sidewalls.

3.4. Flow properties

Numerical simulation is a powerful tool to study the rheology since it allows one to access to more information than experiments. We observed SSHs in both numerical systems we used (FS and PBC; see section 3.2). In FS, when the flow rate exceeds a critical value [14], grains get trapped and the heap forms. A layer of moving grains flows atop a static heap. In PBC, a layer of grains located near the free surface moves as the rest of the medium remains static. This is the case even for very high inclination angles, which is the signature of the SSH in a periodic system. The PBC simulation thus confirms that flows over an SSH are steady and fully developed.

An outstanding result is that both systems give the same relationship between Q and φ, meaning that they are equivalent. If an FS simulation is run with Q_0 as an input, the program outputs a corresponding value of φ_0. When the same value φ_0 is input in the PBC simulation, the program produces the very same flow rate, Q_0.

Figure 15 shows the coordination number and packing fraction profiles averaged over the width and length of the channel, i.e. in the z direction for $W = 20d$ and an angle φ of 45°. An essential new result is that the packing fraction decreases steadily throughout the flowing layer until it nearly vanishes in the agitated surface layer. This is a fundamental difference from granular flows that follow a Bagnold rheology. Silbert [9] and Prochnow [12] show numerically that in a Bagnold flow, the packing fraction stays constant throughout the flow and abruptly decreases when approaching the free surface. Note that such flows are steady and fully developed only for angles that are much lower than in the presence of frictional sidewalls.

Since Silbert [9] and Prochnow [12] simulations are similar to our PBC simulation, except for the absence of the sidewalls, the new regime described here must find its origin in the sidewalls. However, it is not the confinement induced by the sidewalls but the friction on them which is solely responsible for the formation of the SSH. Indeed, when the friction on the sidewalls is turned off (by setting the friction coefficient to zero), our simulations produce Bagnold flows (for angles in the range of $15° < \varphi < 25°$), which are similar to those described in [9]. This shows that the sidewall friction does not simply allow for higher angles for steady flows but also induces fundamental changes in the properties of the flow.

Packing fraction profiles similar to that of figure 14 were observed experimentally by Ancey [18], who studied material flowing directly on the bottom of the cell, but this author did not identify the origin of such a profile. Our simulations can produce such flows (i.e., on the bottom of the cell, with steadily decreasing packing fraction): in PBC (respectively FS), the number of grains (respectively the flow rate) can be chosen to be small enough to prevent

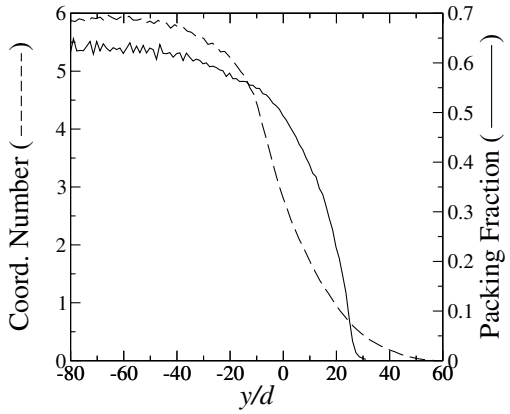

Figure 15. Packing fraction (solid line) and coordination number (dashed line) profiles for a numerical simulation carried out for $W = 20d$ and $\varphi = 45°$.

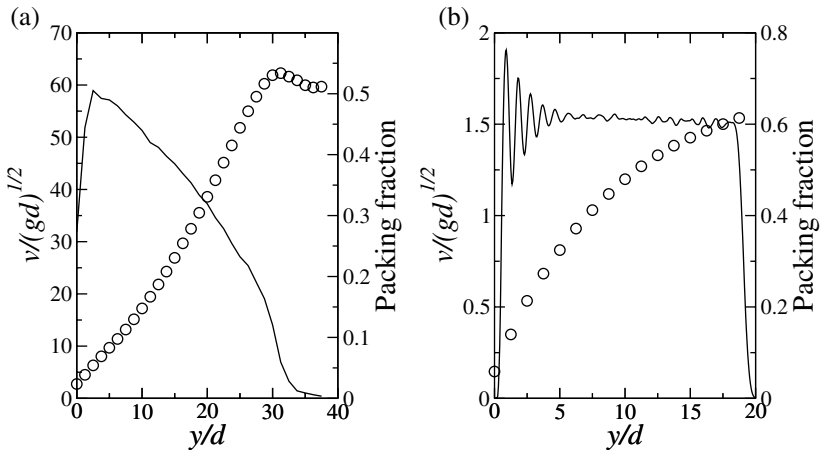

Figure 16. Packing fraction and velocity profiles for flows in a channel between frictional (a) and non-frictional (b) walls. These curves are obtained for $\varphi = 45°$, $W = 20\,d$ and 10 000 grains.

the static part from forming. In this regime, the flow occurs on the bottom of the cell but still depends crucially on friction on the sidewalls, which shows that a steadily decreasing packing fraction profile is not inherent to flow on erodible piles (see figure 16). Note that if the sidewall friction is set to zero, one recovers a Bagnold rheology.

With fundamental changes in the packing fraction profile, one expects to find a rheology different from that of Bagnold. In other words, the relationship between the height of the flow, h, the flow rate, Q, and the angle, φ, should be drastically affected. The linear relationship between φ and h (figure 17(a)) is a reproduction of that found experimentally [14] (see equation (7)). The relationship between Q and h is found to be very different from a Bagnold flow. Figure 17(b) shows that above the jamming transition Q is a linear function of h: $Q \propto (h - h_{\mathrm{jam}})$. This rheology is very different from the Bagnold rheology which predicts a power law, $Q \propto h^{5/2}$, confirmed experimentally for extended flows [7]. As shown in [14], the influence of the sidewalls vanishes when the channel is wide. In this case, one expects the flow to follow a Bagnold rheology.

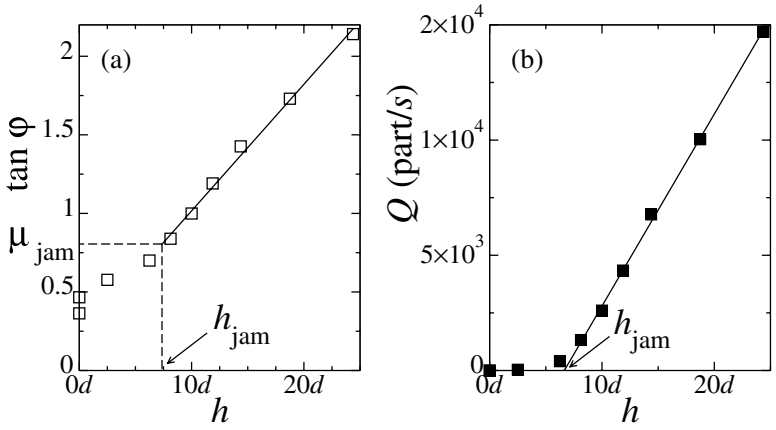

Figure 17. (a) tan φ versus h. The critical value $\mu_{\rm jam}$ found in figure 14 is reported and the corresponding value of h called $h_{\rm jam}$. The solid line shows a linear fit to the curve. (b) Q versus h. Above the critical value $h_{\rm jam}$, Q is a linear function of h. The solid line shows a linear fit to this part of the curve. All the data are obtained using the PBC simulation with $W = 5d$.

In summary, our simulations show that there exist two different flow regimes. Their occurrence depends crucially on the channel width W, the height of the flow h and the sidewall friction. One needs therefore a reliable criterion for predicting the type of flows to occur in a given system. Equation (7) provides us with a dimensionless number, $\xi \equiv (\mu_w h)/(\mu_i W)$, which could furnish a natural criterion. When $\xi \ll 1$, the flow should obey the Bagnold rheology, whereas when $\xi \approx 1$ or $\xi \gg 1$, the flow is expected to obey an SSH rheology with an exponential velocity profile and a decreasing packing fraction. The latter case can be reached by two means: either by increasing the friction coefficient of the sidewalls (which induces an increase of μ_w), or by increasing the height of the flow (i.e. increasing the flow rate). In between these two regimes (when $\xi \lesssim 1$), one observes an intermediate situation where the flow occurs on the rough bottom of the chute, still displaying a decreasing packing fraction. These predictions have to be confirmed by varying the control parameter in extensive numerical simulations.

The flows on SSHs will be extensively analysed in a future paper. However, one can give here some additional features concerning these flows. We show in figure 18 the rotation speed and the temperature profiles averaged along the flow width (i.e., the z direction). One can note that the profile of the rotation speed along the z axis follows qualitatively and quantitatively the same evolution as the shear rate. The rotation speed first increases with y up to a maximum and then decreases. The maximum is located slightly before the beginning of the gaseous part of the flow (see figure 18). One can note also that the granular temperature T_x also behaves in the same manner as the shear rate, indicating that a simple relation between these two quantities should exist. The temperatures along the other directions T_y and T_z (not shown in the figure) present a similar evolution.

4. Conclusion

In conclusion, we have reported on experimental and numerical results on 2D and 3D confined granular chute flows and pointed out the important role of the lateral boundaries. In the 2D configuration where particles are confined between two flat frictional lateral walls, we have

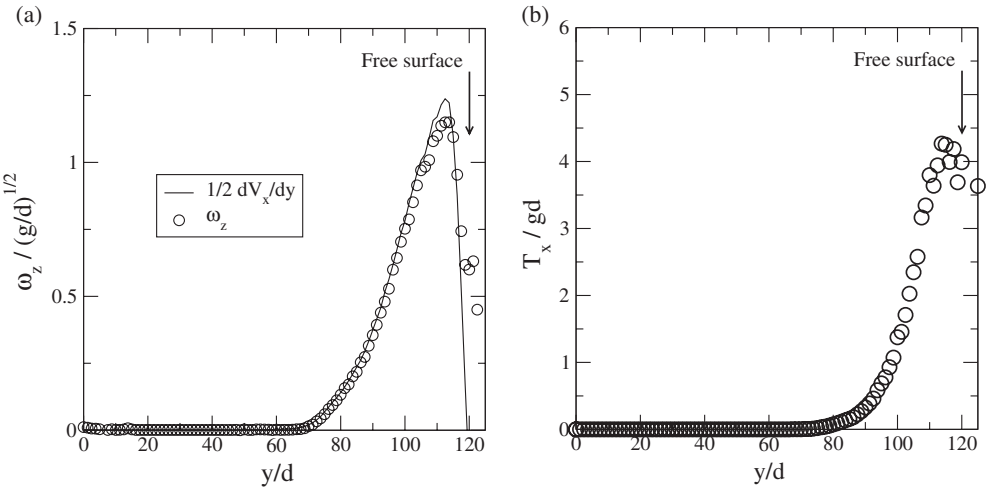

Figure 18. (a) Mean rotation speed along the z axis versus y. Note that the rotation speed was averaged over the flow width. (b) Mean temperature T_x versus y. Here again the temperature was averaged over the flow width. The data were obtained using the PBC simulation with $W = 20d$, $\varphi = 45°$, $N = 60\,000$, $\mu = 0.8$, and $L = 25d$.

seen that SFD flows on rough bottom can be sustained at unusually high inclination angles. The velocity of these flows obeys a Bagnold profile but the flow rate scales with the square of the flow height, contrary to what can be observed in 3D extended flows where $Q \propto h^{5/2}$. We also demonstrated the formation of an SSH at high flow rates. The SSH is stabilized by the flowing layer atop it. These flows atop the SSH exhibit a seemingly linear velocity profile in the bulk flow. In addition, the packing fraction of both flow regimes is found to remain rather constant within the flowing layer.

In 3D confined geometry with flat frictional sidewalls, we recover experimentally and numerically the same phenomenology as in 2D, that is the existence of two different flow regimes, SFD flows on the chute bottom and flows atop the SSH. We showed that these two regimes have completely different flow features. SFD flows on rough bottoms follow a Bagnold velocity profile with a constant packing fraction within the flowing layer, whereas flows atop an SSH exhibit an exponential velocity profile with a decreasing packing fraction. In the latter regime, the flow rate Q scales as $(h - h_{\mathrm{jam}})$ for thick flows but displays a power law behaviour for thin flows (i.e., for $h < 10d$; see figure 17). Thus, if one only considers such thin flows, one would be tempted to conclude that they exhibit a Bagnold-like discharge curve. In addition, we identified a dimensionless parameter, $\xi = \mu_w h/\mu_i W$, which is expected to drive the transition between these two flow regimes. In the crossover regime (i.e., when $\xi \lesssim 1$), flows occur on the bottom of the chute, but still display a decreasing packing fraction profile.

We should emphasize that although purely 2D and 3D confined flows exhibit similar phenomenologies, some marked differences are observed. First, in 2D, SFD flows on rough bottoms slightly deviate from the Bagnold discharge law. This may be due to the fact that in the 2D configuration sidewall friction plays an important role, even in the case of thin flows. Second, the variation of the packing fraction throughout the flow for flows atop an SSH is not confirmed in 2D experiments. At the present moment, we do not have a clear explanation for this discrepancy.

The above results clearly point out the fundamental role of the lateral boundaries on the chute flow features. We have identified the key role of the friction for flat lateral sidewalls but

it would be highly desirable to investigate in the future whether bumpy sidewalls would lead to the same phenomenology. Finally, our results raise a fundamental issue about the existence of steady and fully developed flows on an erodible pile in an extended geometry (i.e., without walls) or in a confined geometry with frictionless sidewalls.

Acknowledgments

We would like to thank G Berton, J T Jenkins, W Losert, M Louge, L Oger and J-M Pasini for helpful discussions, as well as S Bourles for technical assistance. This work was supported by the Centre National de Recherche Scientifique (through 'PNRN' and 'CNRS-NSF' grants) and by the French Ministry of Research (through 'ACI' grants).

References

[1] Jenkins J T and Savage S B 1983 A theory for the rapid flow of identical, smooth, nearly elastic, spherical particles *J. Fluid Mech.* **130** 187
[2] Hungr O and Morgenstern N R 1984 Experiments on the flow behaviour of granular materials at high velocity in an open channel *Géotechnique* **34** 405–13
[3] Drake T G 1990 Structural features in granular flows *J. Geophys. Res.* **95** 8681–96
[4] Johnson P C, Nott P and Jackson R 1990 Frictional–collisional equations of motion for particulate flows and their application *J. Fluid Mech.* **210** 501–35
[5] Azanza E 1998 Two-dimensional granular flows down an inclined plane *PhD Thesis* Ecole Nationale des Ponts et Chaussees, Paris
[6] Azanza E, Chevoir F and Moucheront P 1999 Experimental study of collisional granular flows down an inclined plane *J. Fluid Mech.* **400** 199
[7] Pouliquen O 1999 Scaling laws in granular flows down rough inclined planes *Phys. Fluids* **11** 542–8
[8] Walton O 1993 Numerical simulation of inclined chute flows of monodisperse, inelastic frictional spheres *Mech. Mater.* **16** 239–47
[9] Silbert L E, Ertas D, Grest G S, Halsey T C, Levine D and Plimpton S J 2001 Granular flow down an inclined plane: Bagnold scaling and rheology *Phys. Rev.* E **64** 051302
[10] Silbert L E, Grest G, Plimpton S J and Levine D 2002 Boundary effects and self-organization in dense granular flows *Phys. Fluids* **14** 2637–46
[11] Silbert L E, Landry J W and Grest G S 2003 Granular flow down a rough inclined plane: transition between thin and thick piles *Phys. Fluids* **15** 1
[12] Prochnow M April 2002 Écoulements denses de grains secs *PhD Thesis* ENPC Paris/Marne la Vallée (France)
[13] Midi G D R 2004 On dense granular flows *Eur. Phys. J.* E **14** 341–65
[14] Taberlet N, Richard P, Valance A, Losert W, Pasini J-M, Jenkins J T and Delannay R 2003 Superstable granular heap in a thin channel *Phys. Rev. Lett.* **91** 264301
[15] Taberlet N, Richard P, Henry E and Delannay R 2004 The growth of a super stable heap: an experimental and numerical study *Europhys. Lett.* **68** 515–21
[16] Delannay R, Jenkins J, Louge M, Richard P, Taberlet N and Valance A 2004 Dense granular flows down inclines, under review
[17] Bi W, Richard P, Valance A and Delannay R 2004 Experimental study of two-dimensional granular chute flows of identical circular disks down inclines, under review
[18] Ancey C 2002 Dry granular flows down an inclined channel: experimental investigations on the frictional-collisional regime *Phys. Rev.* E **65** 011304
[19] Jenkins J T and Richman M W 1985 Kinetic theory for plane shear flows of a dense gas of identical, rough, inelastic, circular disks *Phys. Fluids* **28** 3485
[20] Lun C K K and Savage S B 1987 A simple kinetic theory for granular flow of rough, inelastic, spherical particles *J. Appl. Mech.* **54** 47–53
[21] Dippel S 1998 Microscopic dynamics of granular materials *PhD Thesis* Hochstleistungsrechenzentrum Jul-3510
[22] Mitarai N and Nakanishi H 2004 Density profile of dense granular flow down a rough slope *Preprint* cond-mat/0407651 v1
[23] Drake T G 1991 Granular flow: physical experiments and their implications for microstructural theories *J. Fluid Mech.* **225** 121–52
[24] Komatsu T S, Inagaki S, Nakagawa N and Nasuno S 2001 Creep motion in a granular pile exhibiting steady surface flow *Phys. Rev. Lett.* **86** 1757–60

[25] Bonamy D, Daviaud F and Laurent F 2002 Experimental study of granular surface flows via a fast camera: a continuous description *J. Fluid Mech.* **14** 1666–73
[26] Schaefer J, Dippel S and Wolf D E 1996 Force schemes in simulations of granular materials *J. Physique* I **6** 5–20
[27] Falcon E, Laroche C, Fauve S and Coste C 1998 Collision of a 1-d column of beads with a wall *Eur. Phys. J.* B **5** 111–31
[28] Louge M Y and Keast S C 2001 On dense granular flows down flat frictional inclines *Phys. Fluids* **13** 1213–33